THE JOURNAL OF PHYSICAL CHEMISTRY C

Article

pubs.acs.org/JPCC

Visible Light Photoelectrochemical Properties of $PbCrO_4$, Pb_2CrO_5, and Pb_5CrO_8

Heung Chan Lee,[†] Sung Ki Cho,[§] Hyun S. Park,[‡] Ki Min Nam,[⊥] and Allen J. Bard*[,#]

[†]Energy Lab, Samsung Advanced Institute of Technology, Samsung Electronics Co., Ltd., 130 Samsung-ro, Suwon 16678, Republic of Korea

[§]Department of Energy and Chemical Engineering, Kumoh National Institute of Technology, 61 Daehak-ro, Gumi-si, Gyeongsangbuk-do 730-701, Republic of Korea

[‡]Fuel Cell Research Center, Korea Institute of Science and Technology (KIST), Seongbuk-gu, Seoul 02792, Republic of Korea

[⊥]Department of Chemistry, Mokpo National University, 1666 Yeongsan-ro, Cheonggye-myeon, Muan-gun, Jeonnam 58554, Republic of Korea

[#]Center for Electrochemistry, Department of Chemistry and Biochemistry, The University of Texas at Austin, 105 Eest 24th Street, Stop A5300, Austin, Texas 78712, United States

Supporting Information

ABSTRACT: Photoactivities of lead chromates with various combinations of Pb and Cr are rapidly screened using scanning electrochemical microscopy (SECM). In the rapid screening investigation, the metal oxide spot electrode with a Pb/Cr ratio of 2:1 exhibits the highest photoactivity among the semiconductor prepared with different compositions. The photoactivity and electrochemical properties of thin-film electrodes of $PbCrO_4$, Pb_2CrO_5, and Pb_5CrO_8 are further studied following the combinatorial screening. In the bulk electrode measurements, the Pb_2CrO_5 bulk electrode displays the highest photocurrent of 0.23 mA/cm^2 for SO_3^{2-} oxidation at 0.4 V vs Ag/AgCl under 100 mW/cm^2 UV−vis light irradiation. Pb_2CrO_5 presents visible light activity with an absorption wavelength up to 550 nm and an incident photon to current conversion efficiency (IPCE) of 10% at the wavelength of 340 nm. The onset wavelength observed in the UV−vis absorption spectrum increases with increasing Pb contents in lead chromates. Optically obtained direct band gaps decreased from 2.38 to 2.25 to 2.07 eV for $PbCrO_4$, Pb_2CrO_5, and Pb_5CrO_8, respectively. However, the onset wavelength that appeared in IPCE is 2.26 ± 0.02 eV for all three lead chromates where the photocurrent under longer wavelength light irradiation is insignificant. The results imply that more Pb 6s orbitals form interband states, increasing optical transitions in lead chromates. The band structures of $PbCrO_4$, Pb_2CrO_5, and Pb_5CrO_8 are also determined by electrochemical analyses and ultraviolet photoelectron spectroscopy (UPS).

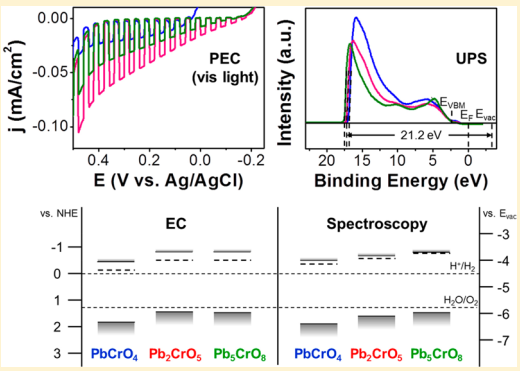

1. INTRODUCTION

Photoelectrochemical (PEC) reactions utilize photons with energy larger than the size of the band gap of the semiconducting electrode. The adsorbed photon generates excited electrons in the conduction band and holes in the valence band, and the electron and hole produced in the electrode are separated by the electric field in the space-charge region and used in the electrochemical reactions.

Finding an efficient photocatalytic semiconductor material that is active to a significant portion of the solar spectrum has been a key step for achieving a feasible light-to-chemical energy conversion system.[1] Wide band gap metal oxides, such as TiO_2, have been widely investigated as a photocatalyst due to the chemical stability and ability to produce high photovoltages. However, the large band gap limits the solar energy conversion efficiency, for example, the theoretical efficiency down to 4% for TiO_2, as only the low fraction of the incidence photon in the UV or short-wavelength visible region can be employed for the PEC reactions. To resolve the low absorption efficiency of large band gap metal oxide electrodes, efforts for band gap modification,[2,3] sensitization,[4] or utilization of new photocatalytic materials with narrower band gaps[5−9] have been conducted.

Various narrow band gap metal oxides with visible light activity have been extensively investigated for PEC applications. Yellow-colored $BiVO_4$ absorbs light up to 520 nm with a 2.4 eV band gap,[10,11] and red-colored Fe_2O_3 absorbs light up to 590 nm with a 2.1 eV band gap.[12] Many of these metal oxide semiconductors have transition metal-centered tetrahedral structures that allows strong electron transition between

Received: April 5, 2017
Revised: June 29, 2017
Published: July 31, 2017

DOI: 10.1021/acs.jpcc.7b03230
J. Phys. Chem. C 2017, 121, 17561−17568

nonbonding O 2p orbitals (t_1) to antibonding orbitals (e) of metal 3d orbitals and O 2p orbitals.[13] Many ternary metal oxides with Cr-centered tetrahedral structures such as $BaCrO_4$ and $SrCrO_4$ are also visible light-active photocatalysts, and their electronic band structures vary with the cations (Ba^{2+} and Sr^{2+}).[14]

In this study, we investigate the PEC properties of lead chromate with different composition ratios between Pb and Cr and explore their electronic band structures as a visible light-active photocatalyst. There are four types of reported oxides in the Pb−Cr−O ternary system: $PbCrO_4$, Pb_2CrO_5, Pb_5CrO_8, and $Pb_{11}CrO_{16}$. Among them, the first three oxides with $Pb(PbO)_nCrO_4$ (n = 0, 1, 4) composition were known to have an optoelectronic property. $PbCrO_4$ is a well-known yellow pigment with a monoclinic $P2_1/n$ structure,[15,16] and possible application of $PbCrO_4$ as an optoelectronic material was reported.[17,18] The photoactivity of $PbCrO_4$ was also reported with insignificant activity for water splitting.[19−21] Pb_2CrO_5 is known as chromium orange with monoclinic structure in space group $c2/m$.[22,23] It was studied as a photoconductive dielectric material with high absorption coefficients in the visible and ultraviolet light spectrum in which its conductivity changes rapidly under the light irradiation.[24−26] Its use as a photovoltaic material was also reported in which 1.16 V of photovoltage was observed with an irradiated light intensity of 23.35 mW/cm^2.[27−29] Pb_5CrO_8 has a monoclinic $P2_1/c$ space group symmetry,[30] and it is a less researched material except for a study of optoelectronic properties as a line-image sensor.[31]

However, to the best of our knowledge, no PEC properties of Pb_2CrO_5 and Pb_5CrO_7 have been reported for photochemical reactions. In this study, we explore the PEC properties of $Pb(PbO)_nCrO_4$ and discuss the electronic band structures of the Cr-centered tetrahedral oxide material with varying PbO contents. Scanning electrochemical microscopy (SECM) was also successfully utilized to conduct a rapid screening study of the photoactivities of lead chromates according to PbO contents. Finally, $PbCrO_4$, Pb_2CrO_5, and Pb_5CrO_8 were fabricated into larger photoelectrodes, and optical and PEC characteristics were reported.

2. EXPERIMENTAL SECTION

Materials. F-doped tin oxide (FTO)-coated glass was purchased from Pilkington (Toledo, OH) and cut into 1.5 cm × 2.0 cm pieces. The cut FTO glasses were cleaned by sonication in an ethanol bath over 40 min and dried overnight in air and then used for spot array substrates as well as thin-film electrode substrates. $Pb(NO_3)_2$ (99.999%, Acros), $Cr(NO_3)_3{\cdot}9H_2O$ (99.99%, Acros), and $K_2Cr_2O_7$ (99.9%, Mallinckrodt) were purchased and used without further purification. Ethylene glycol (certified ACS, Fischer Scientific) was used as the solvent to prepare precursor solutions. All aqueous electrolytes used for electrochemical measurements were prepared using Milli-Q water with a solution resistivity of 18 MΩ·cm.

Preparation of Pb−Cr−O Spot Arrays. Pb−Cr oxide spot arrays for combinatorial screening were prepared by a previously reported procedure.[32−34] Briefly, the metal oxide arrays with varying ratios between Pb and Cr were fabricated by dispensing each 0.1 M $Pb(NO_3)_2$ and 0.1 M $Cr(NO_3)_3{\cdot}9H_2O$ solution in ethylene glycol on a FTO glass substrate in a preprogrammed pattern using a picoliter solution dispenser (model 1550, CH Instruments, Austin, TX). The dispenser was composed of a piezoelectric dispensing tip (MicroJet AB-01-60, MicroFab, Plano, TX) attached to a computer-controlled stepper-motor-operated XYZ stage. Dispensing of a preprogrammed number of drops of the 0.1 M Pb and 0.1 M Cr precursor solution by applying voltage pulses at 80 V for 60 μs to the piezoelectric dispenser resulted in an array of patterns with various compositions of Pb and Cr precursor spots. Then, the arrays were annealed at 500 °C for 3 h with a ramp up rate of 1 °C/min to form oxide spot arrays. The total number of drops was 10, and compositions of Cr and Pb were varied from 10:0 to 0:10, resulting in oxide spots with a diameter of 500 μm on the FTO substrate.

Preparation of Thin-Film Electrodes. Three types of lead chromate polycrystalline thin-film electrodes were fabricated by the drop casting method. For Pb_2CrO_5 and Pb_5CrO_8, a 6 mM $Pb(NO_3)_2$ and 3 mM $Cr(NO_3)_3$ ethylene glycol solution and a 15 mM $Pb(NO_3)_2$ and 3 mM $Cr(NO_3)_3$ ethylene glycol solution were prepared, separately. A volume of 400 μL of each of these premixed solution was drop-cast on the cleaned FTO substrates followed by annealing at 500 °C for 3 h with the ramp rate of 1 °C/min. Prepared Pb_2CrO_5 and Pb_5CrO_8 were orange and reddish orange color, respectively (Figure S1b,c).

For the $PbCrO_4$ thin-film electrode, $PbCrO_4$ powder was produced and coated on the FTO substrate. Briefly, the $PbCrO_4$ powder was synthesized by adding 100 mL of 0.25 M $K_2Cr_2O_7$ aqueous solution slowly into a 500 mL beaker containing 100 mL of 0.5 M $Pb(NO_3)_2$ with vigorous stirring by a magnetic stirrer. Yellow $PbCrO_4$ powder was precipitated immediately and washed with DI water five times. The precipitates were isolated by filter paper (Grade 1, Whiteman) and dried in the drying oven at 110 °C overnight. Then, 0.485 g of the dried $PbCrO_4$ was suspended in 50 mL of ethylene glycol, and 300 μL of the suspension was drop-cast on a cleaned FTO substrate followed by annealing at 200 °C for 3 h in air. The prepared electrode showed bright yellow color (Figure S1a).

Screening of the Arrays. The screening of the photocatalyst arrays is also described in a previous publication.[32] Briefly, a SECM (CHI model 900B, Austin, TX) equipped with an optical fiber replacing an ultramicroelectrode was used to map the photoactivities of the fabricated spot arrays. The optical fiber (FT-400-URT, 3M, St. Paul, MN) was coupled to a 150 W xenon lamp (Oriel, Stratford, CT) to irradiate the spot array electrodes. The Pb−Cr oxide photoelectrodes were mounted in the Teflon cell with a Pt wire counter electrode and a Ag/AgCl reference electrode. In the study, the potential (V) is reported with respect to Ag/AgCl unless otherwise mentioned. Only the array portion of the FTO glass was exposed by a Viton O-ring to the electrolyte of 0.1 M Na_2SO_4 and 0.1 M Na_2SO_3, while on the other side of the FTO, a contact to a copper tape was used for the working electrode connection. The optical fiber was perpendicularly placed 150 μm above the spot array surface and scanned with a speed of 500 μm/s while current from the spot array FTO electrode was recorded at 0.2 V. The measured current with a two-dimensional spatial coordinate results in a color-coded PEC activity map of the spot arrays.

Photoelectrochemistry of the Bulk Electrode. A conventional three-electrode borosilicate glass cell with a 0.25 cm^2 diameter window for thin-film photoanode mounting was used for PEC analysis. An O-ring with a 0.27 cm^2 inner diameter was used to seal between the cell and photoanode, by which the surface area of the photoelectrode was defined. A Pt wire and a Ag/AgCl electrode were used as the counter electrode and the reference electrode, respectively. All electro-

DOI: 10.1021/acs.jpcc.7b03230
J. Phys. Chem. C 2017, 121, 17561−17568

chemical measurements were conducted in a 0.1 M Na_2SO_3 and 0.1 M Na_2SO_4 solution. Na_2SO_3 was used as a sacrificial electron donor to investigate the PEC properties with minimized surface recombination and photodecomposition. All DC electrochemical measurements were conducted using a CHI630 potentiostat (CH Instrument, TX). The photoelectrodes were irradiated by a 150 W Xe lamp with a power density of 100 mW/cm^2 at the electrode surface. Visible light was irradiated by placing the 420 nm low-pass filter in front of the lamp. To obtain the action spectrum, a monochromator (Oriel) was used to irradiate light with specific wavelengths. Mott−Schottky plots of the thin-film electrodes were obtained by conducting electrochemical impedance spectroscopy (EIS) using an Autolab PGSTAT128N (Metrohm USA, Inc.) in a 0.1 M Na_2SO_4 solution. An AC amplitude of 10 mV at three different frequencies (200, 500, and 1000 Hz) was used for the impedance measurements.

Material Characterization. The crystalline phases of the electrodes were characterized by X-ray diffraction (XRD, D8, Bruker-Nonius, WI) operated at 40 kV and 40 mA with Cu Kα radiation (λ = 1.54 Å). The scan rate was 12° per minute in 0.02° increments of 2θ from 15 to 80°. A scanning electron microscope (SEM, Quanta 650 FEG, FEI Company, Inc., Hillsboro, OR) was also used to observe the surface morphology of prepared film electrodes. UV−vis light absorbance of the prepared electrodes was measured using a UV−vis NIR spectrometer (Cary 5000, Agilent, CA) with an integrating sphere and a center mount sample holder. The band structures of Pb_2CrO_5, Pb_5CrO_8, and $PbCrO_4$ were also analyzed via ultraviolet photoelectron spectroscopy (UPS) measurement (PHI 5000 VersaProbe, ULVAC PHI, Japan). UPS spectra were measured using He I excitation (21.2 eV) and recorded with a constant pass energy of 0.585 eV in the ultrahigh vacuum (UHV) chamber. To ensure that the secondary electron cutoff was captured, a sample bias of −9 V was applied to compensate for the instrument work function difference repelling low kinetic energy electrons. Before the measurement, the surface contaminants were removed by Ar^+ sputtering (3 kV) for 1 min.

3. RESULTS AND DISCUSSION

Rapid Screening of the Pb−Cr−O System in SECM. To investigate the PEC activity of the lead chromate compounds, microelectrode spot arrays containing a preprogrammed ratio of Pb and Cr were fabricated and annealed to form lead chromate spots on a FTO substrate, as described above. A total of 11 spots were formed on one FTO substrate, and each spot had a Pb and Cr ratio from 10:0 to 0:10. The ratio of the contents is illustrated in Figure 1a. The spot arrays were rapidly scanned in the SECM to access the photooxidation current regarding the semiconductor compositions. Figure 1b represents the SECM image of the Pb−Cr−O spot arrays when UV−vis light is irradiated via the optical fiber. The potential of the electrode substrate was held at 0.2 V. The brightest spot and the second brightest spot corresponded to Pb and Cr ratios of 7:3 and 6:4 with sulfite oxidation currents of approximately 50 and 39 nA, respectively, whereas nonactive compounds showed background current, , that is, 30 nA in Figure 1b. The result represents promising photoactivities at Pb-rich spots with reference to the 5:5 spot, which corresponds to $PbCrO_4$. The Pb−Cr−O oxide with a Pb and Cr ratio between 7:3 and 6:4 could correspond to Pb_2CrO_5. Therefore, thin films of

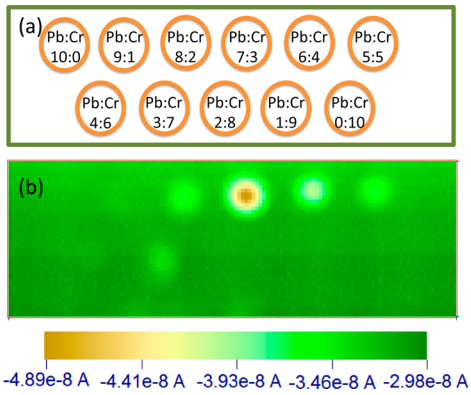

Figure 1. (a) Schematic diagram of the array pattern and number of drops of each 0.1 M Pb and Cr ethylene glycol solution. (b) SECM image of the Pb−Cr−O spot arrays at 0.2 V vs Ag/AgCl with UV−vis irradiation in the 0.1 M Na_2SO_3 and 0.1 M Na_2SO_4 solution. The size of the array was 6400 × 2400 μm, and the scan rate was 500 μm/s.

$Pb(PbO)_nCrO_4$ (n = 1, 2, 4) were fabricated for deeper investigation.

Photoelectrochemistry of Thin-Film Electrodes. To verify the result of combinatorial screening of the Pb−Cr−O system, $PbCrO_4$, Pb_2CrO_5 and Pb_5CrO_8 thin-film electrodes were prepared to study the physical and electrochemical properties of the photoelectrodes. XRD patterns in Figure S2 confirm that the crystalline structures of Pb_2CrO_5, Pb_5CrO_8, and $PbCrO_4$ are phoenicochroite (Pb_2CrO_5, PDF #84-0678), lead chromium oxide (Pb_5CrO_8, PDF #47-0678), and crocoite ($PbCrO_4$, PDF #47-2304), respectively. SEM images also reveal that fabricated $PbCrO_4$ crystals on FTO are micron-size rod-shaped, while both Pb_2CrO_5 and Pb_5CrO_8 are micron-size particles, as presented in Figure S2. The film morphologies can also influence the light absorption, carrier separation and diffusion and, consequently, the photoactivities. PEC analysis of single crystals with proper contacts will provide unambiguous photoactivities at particular crystalline surfaces. However, it is beyond the scope of this research and left for a future work.

A sacrificial electron donor, Na_2SO_3, was used to observe PEC performance of the semiconducting electrodes without significant surface recombination or side reactions. The photooxidation of SO_3^{2-} to SO_4^{2-} is kinetically facile, with insignificant photoinduced side reactions such as photodecomposition or surface recombination. Figure 2 shows the linear sweep voltammograms (LSVs) of $PbCrO_4$ (blue), Pb_2CrO_5 (red), and Pb_5CrO_8 (green) under UV−vis light (a) and visible light (b). The potential was swept from 0.25 to −0.5 V at a scan rate of 20 mV/s with chopped light irradiation in 0.1 M Na_2SO_3 and 0.1 M Na_2SO_4 aqueous solution purged with Ar. A fast increase and decrease of the photocurrent was observed when the light was turned on and off. In the presence of the sacrificial reagent, no sign of transient photocurrent decay due to surface recombination was observed in LSVs. The photocurrents under UV−vis irradiation at 0.4 V are shown for different lead chromates in Figure 2c. Pb_2CrO_5 has the highest photocurrent of 0.22 mA/cm^2, which is in agreement with the screening result and is approximately 7 times higher than the photocurrent of $PbCrO_4$ (0.03 mA/cm^2) and 3.5 times higher than the photocurrent of Pb_5CrO_8 (0.06 mA/cm^2). Under visible light irradiation, a photocurrent of 0.07 mA/cm^2 was measured for Pb_2CrO_5 at 0.4 V, which is also several times higher than those of $PbCrO_4$ and Pb_5CrO_8. Dark background

DOI: 10.1021/acs.jpcc.7b03230
J. Phys. Chem. C 2017, 121, 17561−17568

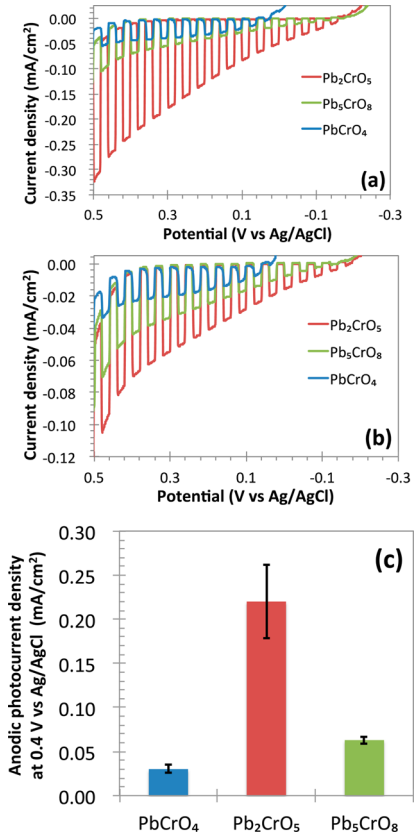

Figure 2. LSVs of $PbCrO_4$ (blue), Pb_2CrO_5 (red), and Pb_5CrO_8 (green) in 0.1 M Na_2SO_4 and 0.1 M Na_2SO_3 aqueous solution with intermittent (a) UV–vis light and (b) visible light irradiation. The power density of the UV–vis light was 100 mW/cm^2, and for visible light irradiation, the 420 nm low band path filter is used. The exposed electrode area was 0.27 cm^2. (c) Anodic photocurrents by 100 mW/cm^2 UV–vis light with error bars at 0.4 V in 0.1 M Na_2SO_4 and 0.1 M Na_2SO_3 aqueous solution.

currents for all electrodes starting at 0.4 V were observed due to the oxidation of SO_3^{2-} on the exposed FTO surface as the SEM images in Figure S3 show the exposed FTO surface on these thin-film electrodes. The high photocurrent of Pb_2CrO_5 might originate from its high photoconductivity, whereas the decrease in the photocurrent of Pb_5CrO_8 might be due to the decreased CrO_4^{2-} mole contents compared to that in Pb_2CrO_5 as the increased distance between tetrahedral CrO_4^{2-} resulting in inefficient electron–hole separation.

Absorbance. The activity of the photoelectrodes is determined by three factors, that is, light absorption, electron–hole separation and transport, and surface reaction kinetics for the desired chemical reactions. The light absorption at the photoelectrode determines the theoretical limit of the obtainable photocurrent and can be estimated using the size of the band gap energy (E_g) of the semiconductor electrode. In Figure 3, the transreflectance (TR), transmittance (T) plus reflectance (R), measurements were used to obtain the absorbance.[35] Using the center mount in the integrating sphere, simultaneous measurement of the T and R was performed, and the absorbance was calculated from the following the equation.[35]

$$\text{Absorbance } (A) = -\log(\text{TR}) \tag{1}$$

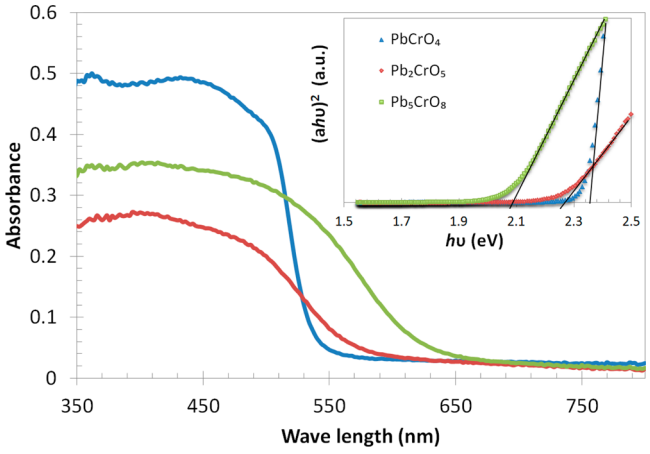

Figure 3. Absorbance of $PbCrO_4$ (blue), Pb_2CrO_5 (red), and Pb_5CrO_8 (green) thin-film electrodes measured in an integrating sphere with a center mount sample holder. The inset shows Tauc plots $((\alpha h\nu)^{1/m}$ vs $h\nu)$ when m = 0.5. The x-intercept of the linear region of the plot indicates an optically obtained direct band gap, 2.38, 2.25, and 2.07 eV for $PbCrO_4$, Pb_2CrO_5, and Pb_5CrO_8, respectively.

Figure 3 shows the absorbance spectrum of Pb_2CrO_5 (red), $PbCrO_4$ (blue), and Pb_5CrO_8 (green) obtained from the TR measurements. Yellow-colored $PbCrO_4$ shows strong absorbance up to approximately 550 nm. The orange-colored Pb_2CrO_5 and reddish orange-colored Pb_5CrO_8 show absorbance up to approximately 600 and 650 nm, respectively. E_g values of crystalline semiconductors were determined from absorbance measurements using the equation below, assuming that the bottom of the conduction band and the top of the valence band are parabolic[36,37]

$$\alpha = B(h\nu - E_g)^m/h\nu \tag{2}$$

where B is a proportional constant, α is the absorption coefficient, h is Planck's constant (J s), ν is the frequency of monochromic light (s^{-1}), and m determines the nature of the band structure. m is 1/2 for a direct band gap where an electron transition from the valence band to conduction band by light absorption occurs without a momentum change. On the other hand, m is 2 for an indirect band gap semiconductor where the momentum changes with the transition. Using eq 2, the size of the optical band gap is obtained at the x-intercept of the extrapolated linear region of the Tauc plot, or $(\alpha h\nu)^{1/m}$ vs $h\nu$. Tauc plots of $PbCrO_4$, Pb_2CrO_5, and Pb_5CrO_8 shown in the Figure 3 inset exhibit broad linear regions with m = 1/2, indicating a direct band gap with band gap sizes of 2.38, 2.25, and 2.07 eV for $PbCrO_4$, Pb_2CrO_5, and Pb_5CrO_8, respectively. The resulting band gap nature and the change in the gap size were consistent with those in previous reports.[38]

IPCE and PEC Measurements. Incident photon to current conversion efficiencies (IPCE) of $PbCrO_4$, Pb_2CrO_5, and Pb_5CrO_7 were obtained to display the ratio between the photocurrent, that is, collected electrons, and the number of irradiated photons (Figure 4). IPCEs were calculated from the action spectrum and the power spectrum of the incident light (Figures S4 and S5, respectively), measured at 0.3 V Ag/AgCl under monochromatic light irradiation. Figure 4a shows IPCE plots of the three thin-film electrodes over a wavelength range of 300–650 nm calculated with the following equation

$$\text{IPCE } (\%) = 1240 \times (j_{ph}/\lambda P_{in}) \times 100 \tag{3}$$

DOI: 10.1021/acs.jpcc.7b03230
J. Phys. Chem. C 2017, 121, 17561–17568

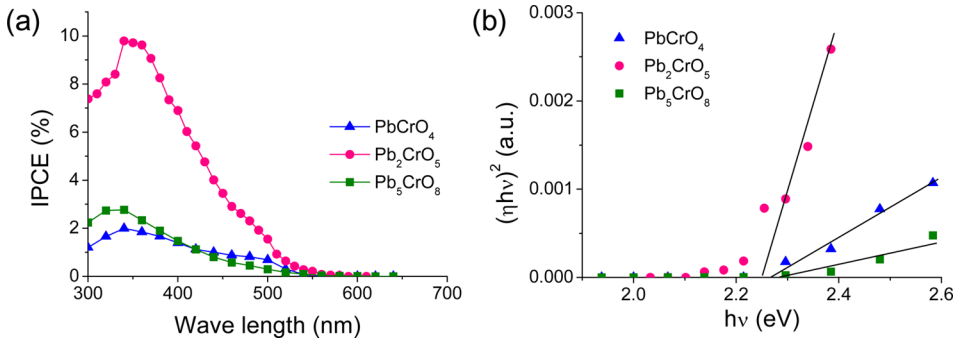

Figure 4. (a) IPCE plots and (b) Tauc plots $((\eta h\nu)^{1/m}$ vs $h\nu$, when $m = 1/2$ are shown) of $PbCrO_4$ (blue), Pb_2CrO_5 (red), and Pb_5CrO_8 (green). The photocurrents at each wavelength were measured at 0.3 V vs Ag/AgCl in 0.1 M Na_2SO_4 and 0.1 M Na_2SO_3 aqueous solution. In the Tauc plot, the x-intercept of the linear region of the plot indicates a direct band gap, 2.26, 2.24, and 2.28 eV for $PbCrO_4$, Pb_2CrO_5, and Pb_5CrO_8, respectively.

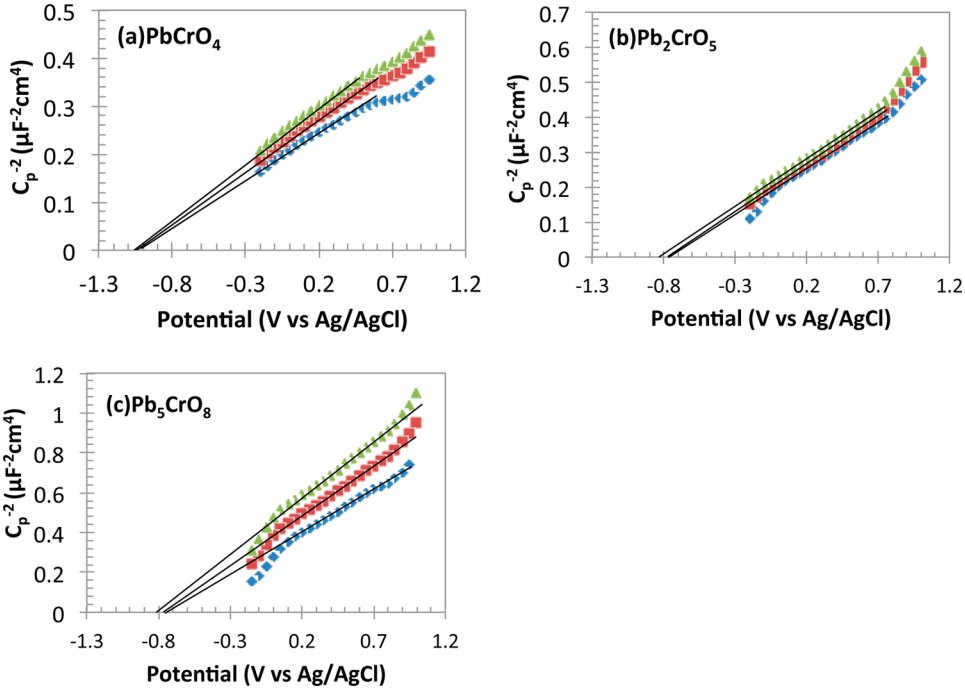

Figure 5. M–S plots of (a) $PbCrO_4$, (b) Pb_2CrO_5, and (c) Pb_5CrO_8 obtained from the AC impedance capacitance measurements in 0.1 M phosphate buffer and 0.1 M $NaSO_4$ solution. An AC amplitude of 10 mV was applied for each potential, and three different AC frequencies were used for the measurements: 1000 (green), 500 (red), and 100 Hz (blue). Tangent lines of the M–S plots are drawn to obtain the flat band potential.

where j_{ph} is the photocurrent density (mA/cm^2), λ is the wavelength (nm), and P_{in} is the incident light power density (mW/cm^2). For Pb_2CrO_5, an IPCE of approximately 10% was observed at 340 nm, while only 3 and 2% were detected for Pb_5CrO_8 and Pb_2CrO_5 at the same wavelength. The band gaps of semiconductors can also be estimated from the following equation using the IPCE measurements[12,39]

$$\mathrm{IPCE} = \eta_{e-h} \times \eta_{trans} \times C(h\nu - E_g)^m/h\nu \quad (4)$$

where η_{e-h} and η_{trans} are the electron–hole separation and surface charge transfer efficiency, respectively. C is the proportionality constant for light absorption at the photoelectrode. If η_{e-h} and η_{trans} are independent of the light absorption or incident light wavelength, the size of the band gap can be obtained using eq 4. For direct band gap semiconductors, the band gap energy is estimated with $m = 1/2$ in eq 4, as shown in Figure 4b. Obtained band gaps using IPCE measurements are approximately 2.26, 2.24, and 2.28 eV for $PbCrO_4$, Pb_2CrO_5, and Pb_5CrO_8, respectively. Photoelectrochemically obtained band gaps of $PbCrO_4$ and Pb_5CrO_8 are largely different from those measured by UV–vis spectroscopy; the size of the band gap estimated in Tauc plots (Figure 3) was 2.38 and 2.07 eV for $PbCrO_4$ and Pb_5CrO_8, respectively. The discrepancy between band gaps obtained from IPCE and UV–vis spectroscopy might originate from the inaccurate measurements of low IPCE, including the inefficient bulk charge separation and surface charge transfer efficiency of the photoelectrodes.

The flat band potential (E_{fb}) of semiconductors can be assessed by measuring the space-charge capacitance of photoelectrodes using EIS. The relationship between the space-charge capacitance and potential in semiconductors follows the Mott–Schottky (M–S) equation, as follows

$$\frac{1}{C^2} = \frac{2}{\varepsilon_s \varepsilon_0 e N_D}\left(E - E_{fb} - \frac{K_B T}{e}\right) \quad (5)$$

where C is the space charge capacitance (F cm^{-2}), ε_s is the relative dielectric constant of the semiconductor, ε_0 is

DOI: 10.1021/acs.jpcc.7b03230
J. Phys. Chem. C 2017, 121, 17561–17568

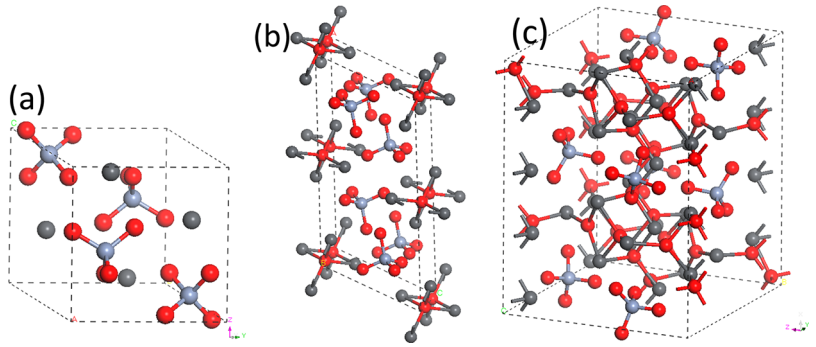

Figure 6. Crystal structures of (a) $PbCrO_4$, (b) Pb_2CrO_5, and (c) Pb_5CrO_8. Light gray, dark gray, and red represent Cr, Pb, and O, respectively. All structures have isolated tetrahedral CrO_4^{2-} with a Cr−O bond length of 1.65 Å surrounded by $Pb(PbO)_n$ (n = 0, 1, 4). XRD crystallographic data are shown in Figure S2.

permittivity of free space (F cm^{-1}), N_D is the majority carrier density (cm^{-3}), k_B is the Boltzmann constant (eV K^{-1}), T is the temperature (K), and E is the applied potential (V). By plotting a $1/C^2$ vs V graph, the x-intercept of the linear portion of the M−S plot is the estimated E_{fb},[40] while the slope of the straight line, that is, $2/(\varepsilon_s\varepsilon_0 eN_D)$, is related to the carrier concentration. Figure 5 represents the M−S plots for (a) $PbCrO_4$, (b) Pb_2CrO_5, and (c) Pb_5CrO_8 in 0.1 M phosphate buffer and 0.1 M $NaSO_4$ solution. An AC amplitude of 10 mV was applied for each potential, and 1000 (green), 500 (red), and 100 Hz (blue) AC frequencies were used for the measurements. Tangent lines of the M−S plots are drawn to obtain the E_{fb}. The positive slope of the M−S plots confirms the n-type doping, and the estimated E_{fb} values were −0.75 V for both Pb_2CrO_5 and Pb_5CrO_8 and −1.1 V for $PbCrO_4$. N_D values calculated from the slope of the respective M−S plot using an ε_s value of 14.9[24] are 3.5 ± 0.1 × 10^{19}, 2.0 ± 0.3 × 10^{19}, and 5.3 ± 0.3 × 10^{19} cm^{-3} for Pb_2CrO_5, Pb_5CrO_8, and $PbCrO_4$, respectively. The carrier densities in three lead chromates seem to be similar, but the actual surface area and ε_s of the porous semiconductor films should be considered to obtain more accurate N_D values.

Band Structures. Crystal structures of $PbCrO_4$ (monoclinic, $P2_1/n$),[41] Pb_2CrO_5 (monoclinic, $c2/m$),[22] and Pb_5CrO_8 (monoclinic, $P2_1/c$)[30] are shown in Figure 6. Light gray, dark gray, and red represent Cr, Pb, and O, respectively. In these three lead chromate structures, tetrahedral CrO_4^{2-} ions are isolated and surrounded by $Pb(PbO)_n^{2+}$ (n = 0, 1, 4).[30] The average bond length of Cr−O in each crystal structure is consistent at 1.65 Å.[22,30,41] It is generally known for $PbCrO_4$ that the bottom of the conduction band consists of an antibonding interaction of Cr 3d and O 2p orbitals, whereas the top of the valence band consists of Pb 6s and O 2p nonbonding orbitals.[42,43] Increased Pb contents might increase Pb 6s character at the top of the valence band, creating sub-band gap states resulting in decreasing the optical band gap from 2.38 eV for $PbCrO_4$ to 2.25 and 2.07 eV for Pb_2CrO_5 and Pb_5CrO_8.

The band structure and the change in the valence band position (E_{fb}, valence band edge) with the increased Pb contents were probed via UPS analysis (Figure 7). UPS measurement has been also successfully utilized for analysis of the change in the valence band of Ta_2O_5 with the substitution of nitrogen for oxygen.[44] In the UPS spectrum, the secondary electron cutoff energy was positively shifted with the increase of Pb contents, indicated by the rise in the Fermi level (E_F) (Figure 7b), whereas the energy level for the valence band maximum (E_{VBM}) with respect to E_F was almost similar (Figure 7c). Consequently, E_{VBM} with respect to the vacuum level (E_{vac})

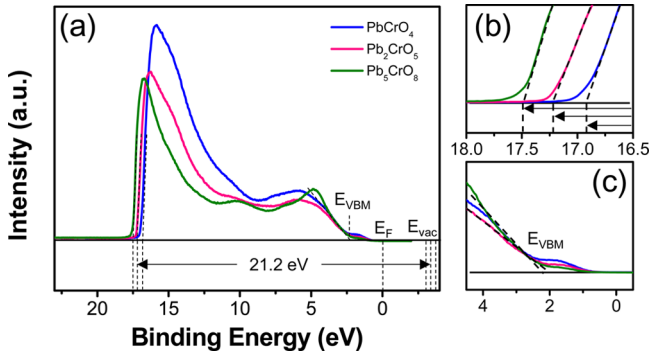

Figure 7. UPS spectrum for $PbCrO_4$ (blue), Pb_2CrO_5 (red), and Pb_5CrO_8 (green): (a) full region, (b) secondary electron cutoff region, and (c) near-Fermi region.

rose with the increase in Pb contents, as expected. The small prepeaks near 1.5 eV in the Fermi edge region (Figure 7c) might originate from the surface defects of oxygen vacancies caused by Ar^+ bombardment as the same peak was also addressed in the UPS spectrum of TiO_2.[45]

The band gap energy, E_F, and band positions of $PbCrO_4$, Pb_2CrO_5, and Pb_5CrO_8 estimated in electrochemical and spectroscopic analyses are summarized in Table 1 and illustrated in Figure 8. E_{fb} measured at pH 7 in M−S plots is reported with respect to the normal hydrogen electrode (NHE) in Figure 8, assuming −59 mV of potential drop at the Helmholtz layer per unit pH.[44] In addition, the conduction band edge (E_{CB}) was estimated with an energy gap of 0.2 eV between E_{fb} and E_{CB}. For the energy gap, high N_D values in typical n-type semiconductors were assumed because precise measurements of N_D are rarely possible on polycrystalline films due to surface capacitance and defects.[44,46] Two different analyses, electrochemical and optical measurements, resulted in quite similar band positions for $PbCrO_4$, Pb_2CrO_5, and Pb_5CrO_8, and both showed a rise in the valence band position with an increase in Pb contents.

4. CONCLUSIONS

In this study, the photoactivities of various compositions of Pb−Cr−O were investigated using the SECM rapid screening method, and Pb_2CrO_5 was found to be the best photocatalyst among them. Thin-film electrodes of $PbCrO_4$, Pb_2CrO_5, and Pb_5CrO_8 were fabricated to verify their PEC properties and optical properties. Pb_2CrO_5 showed a 0.23 mA/cm^2 photocurrent under UV−vis light and 0.06 mA/cm^2 under visible

DOI: 10.1021/acs.jpcc.7b03230
J. Phys. Chem. C 2017, 121, 17561−17568

Table 1. Band Energies of $PbCrO_4$, Pb_2CrO_5, and Pb_5CrO_8 Determined by Electrochemical and Spectroscopic Analyses

	electrochemical analysis				spectroscopic analysis			
eV (vs E_{vac})	E_g	E_F	E_{CB}	E_{VB}	E_g	E_F	E_{CB}	E_{VB}
$PbCrO_4$	2.26	−4.36	−4.16	−6.42	2.38	−4.14 ± 0.17	−4.01 ± 0.20	−6.39 ± 0.20
Pb_2CrO_5	2.24	−4.01	−3.81	−6.05	2.25	−3.94 ± 0.03	−3.85 ± 0.03	−6.10 ± 0.03
Pb_5CrO_8	2.28	−4.01	−3.81	−6.09	2.07	−3.73 ± 0.04	−3.90 ± 0.06	−5.97 ± 0.06

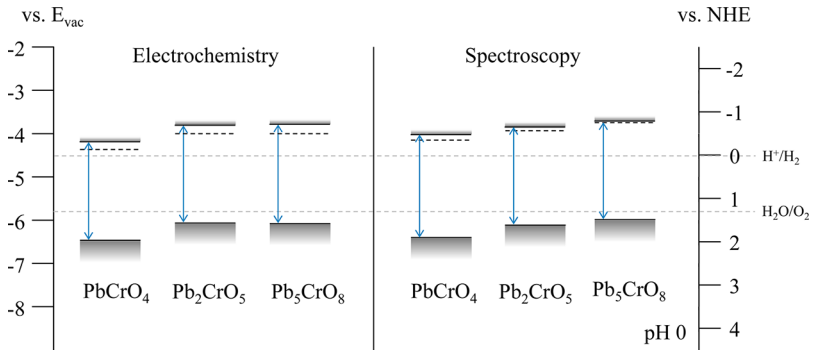

Figure 8. Illustration of band positions of $PbCrO_4$, Pb_2CrO_5, and Pb_5CrO_8 determined by electrochemical and spectroscopic analyses.

light for SO_3^{2-} oxidation. From the action spectrum, visible light activity up to 550 nm was confirmed with 10% IPCE at 340 nm for Pb_2CrO_5. The onsets of the visible light absorption increased as Pb contents increased in the lead chromates probably due to the increased Pb 6s orbitals at the top of the valence band.

■ ASSOCIATED CONTENT

Supporting Information

The Supporting Information is available free of charge on the ACS Publications website at DOI: 10.1021/acs.jpcc.7b03230.

Pictures, SEM images, XRD, action spectra of $PbCrO_4$, Pb_2CrO_5, and Pb_5CrO_8, incident light power spectrum, absorbed photon to current conversion efficiency, and stability tests (PDF)

■ AUTHOR INFORMATION

Corresponding Author

*E-mail: ajbard@mail.utexas.edu. Phone: 512-471-3761. Fax: 512-471-0088.

ORCID

Heung Chan Lee: 0000-0002-1735-6308
Sung Ki Cho: 0000-0002-5173-8625
Allen J. Bard: 0000-0002-8517-0230

Notes

The authors declare no competing financial interest.

■ ACKNOWLEDGMENTS

The authors gratefully acknowledge the U.S. Department of Energy SISGR (DE-FG02-09ER16119) and the Robert A. Welch Foundation (F-0021); a Fondazione Oronzio e Niccolò De Nora Fellowship in Applied Electrochemistry is also gratefully acknowledged. H.S.P. acknowledges support from the National Research Foundation of Korea (2016M3D1A1021142) funded by the Ministry of Science, ICT & Future Planning. H.C.L. thanks Dr. Dongmin Im for valuable discussion and support.

■ REFERENCES

(1) Chen, X.; Shen, S.; Guo, L.; Mao, S. S. Semiconductor-Based Photocatalytic Hydrogen Generation. *Chem. Rev.* **2010**, *110*, 6503−70.

(2) Chen, X.; Liu, L.; Yu, P. Y.; Mao, S. S. Increasing Solar Absorption for Photocatalysis with Black Hydrogenated Titanium Dioxide Nanocrystals. *Science* **2011**, *331*, 746.

(3) Hoang, S.; Guo, S.; Hahn, N. T.; Bard, A. J.; Mullins, C. B. Visible Light Driven Photoelectrochemical Water Oxidation on Nitrogen-Modified TiO_2 Nanowires. *Nano Lett.* **2012**, *12*, 26−32.

(4) O'Regan, B.; Grätzel, M. A Low-Cost, High-Efficiency Solar Cell Based on Dye-Sensitized Colloidal TiO_2 Films. *Nature* **1991**, *353*, 737−740.

(5) Wang, S.; Swingle, S. F.; Ye, H.; Fan, F. F.; Cowley, A. H.; Bard, A. J. Synthesis and Characterization of a p-Type Boron Arsenide Photoelectrode. *J. Am. Chem. Soc.* **2012**, *134*, 11056.

(6) Ida, S.; Yamada, K.; Matsunaga, T.; Hagiwara, H.; Matsumoto, Y.; Ishihara, T. Preparation of p-Type $CaFe_2O_4$ Photocathodes for Producing Hydrogen from Water. *J. Am. Chem. Soc.* **2010**, *132*, 17343−17345.

(7) Ye, H.; Park, H. S.; Bard, A. J. Screening of Electrocatalysts for Photoelectrochemical Water Oxidation on W-Doped $BiVO_4$ Photocatalysts by Scanning Electrochemical Microscopy. *J. Phys. Chem. C* **2011**, *115*, 12464−12470.

(8) Jang, J. S.; Lee, J.; Ye, H.; Fan, F.-R. F.; Bard, A. J. Rapid Screening of Effective Dopants for Fe_2O_3 Photocatalysts with Scanning Electrochemical Microscopy and Investigation of Their Photoelectrochemical Properties. *J. Phys. Chem. C* **2009**, *113*, 6719−6724.

(9) Yourey, J. E.; Bartlett, B. M. Electrochemical Deposition and Photoelectrochemistry of $CuWO_4$, a Promising Photoanode for Water Oxidation. *J. Mater. Chem.* **2011**, *21*, 7651.

(10) Kudo, A.; Omori, K.; Kato, H. A Novel Aqueous Process for Preparation of Crystal Form-Controlled and Highly Crystalline $BiVO_4$ Powder from Layered Vanadates at Room Temperature and Its Photocatalytic and Photophysical Properties. *J. Am. Chem. Soc.* **1999**, *121*, 11459−11467.

(11) Park, Y.; McDonald, K. J.; Choi, K.-S. Progress in Bismuth Vanadate Photoanodes for Use in Solar Water Oxidation. *Chem. Soc. Rev.* **2013**, *42*, 2321−37.

(12) Khan, S. U. M.; Akikusa, J. Photoelectrochemical Splitting of Water at Nanocrystalline n-Fe_2O_3 Thin-Film Electrodes. *J. Phys. Chem. B* **1999**, *103*, 7184−7189.

(13) Woodward, P. M.; Mizoguchi, H.; Kim, Y.; Stoltzfus, M. W. In *Metal Oxides Chemistry and Applications*; Fierro, J. L. G., Ed.; CRC Press: New York, 2006; pp 133−166.

DOI: 10.1021/acs.jpcc.7b03230
J. Phys. Chem. C 2017, 121, 17561−17568

(14) Yin, J.; Zou, Z.; Ye, J. Photophysical and Photocatalytic Properties of New Photocatalysts $MCrO_4$ (M = Sr, Ba). *Chem. Phys. Lett.* **2003**, *378*, 24−28.
(15) Gu, L.; Cao, L.; Meng, G. Formation and Transition of the Phases in the Pb−Cr−O System. *J. Alloys Compd.* **2009**, *474*, 297−300.
(16) Brandt, K. In *Industrial Inorganic Pigments*; Buxbaum, G., Pfaff, G., Eds.; WILEY-VCH: Morlenbach, Germany, 2005; p 128.
(17) Devi, S.; Prakash, S. G. Photoconductivity Studies of ($PbCrO_4$-HgO-ZnO) Composites. *Pramana* **1994**, *43*, 245−253.
(18) Goldman, J. E.; Lawson, A. W. The Photo-Conductivity of Lead Chromate. *Phys. Rev.* **1943**, *64*, 11.
(19) Kudo, A.; Steinberg, M.; Bard, A. J.; Campion, A.; Fox, M. A.; Mallouk, T. E.; Webber, S. E.; White, J. M. Photoactivity of Ternary Lead-Group IVB Oxides for Hydrogen and Oxygen Evolution. *Catal. Lett.* **1990**, *5*, 61−66.
(20) Davidson, R. S.; Willsher, C. J. The Electrochemical Behaviour of Light-Sensitive Electrodes Formed by Coating a Platinum Mesh with a Powdered Semiconductor. *J. Appl. Electrochem.* **1982**, *12*, 517−523.
(21) Miseki, Y.; Kitao, O.; Sayama, K. Photocatalytic Water Oxidation over $PbCrO_4$ with 2.3 eV Band Gap in IO_3^-/I^- Redox Mediator under Visible Light. *RSC Adv.* **2015**, *5*, 1452−1455.
(22) Morita, S.; Toda, K. Determination of the Crystal Structure of Pb_2CrO_5. *J. Appl. Phys.* **1984**, *55*, 2733.
(23) Ruckman, J. C.; Morrison, R. T. W.; Buck, R. H. Structure and Lattice Parameters of Dilead(II) Pentaoxochromate(VI). *J. Chem. Soc., Dalton Trans.* **1972**, *0*, 426−427.
(24) Toda, K.; Yoshida, S.; Ikenaga, H. Current-Voltage Characteristics of an Au/Pb_2CrO_5/Cr Sandwiched-Structure Device. *J. Mater. Sci. Lett.* **1993**, *12*, 478−479.
(25) Toda, K.; Abdul-Gader, M. M.; Okada, M. Impedance Analysis of the AC Behaviour of a Au/Pb_2CrO_5/SnO_2 Thin-Film Device. *J. Phys.: Condens. Matter* **1997**, *9*, 3609.
(26) Araújo, V. D.; Avansi, W.; Paris, E. C.; Maia, L. J. Q.; Bernardi, M. I. B. Influence of pH on the Incorporation and Growth of Pb_2CrO_5 Crystallites in Silica Matrix. *J. Sol-Gel Sci. Technol.* **2011**, *59*, 488−494.
(27) Toda, K.; Yoshida, S. Photovoltaic Mechanism of Pb_2CrO_5 Ceramic Disk with a Pair of Planar Electrodes. *J. Appl. Phys.* **1988**, *63*, 1580−1584.
(28) Toda, K.; Morita, S. Optical Properties and Photovoltaic Effect in Pb_2CrO_5 Thin Films. *J. Appl. Phys.* **1985**, *57*, 5325.
(29) Toda, K.; Morita, S. Determination of the Crystal Structure of Pb_2CrO_5. *J. Appl. Phys.* **1984**, *55*, 210.
(30) Krivovichev, S. V.; Armbruster, T.; Depmeier, W. Crystal Structures of $Pb_8O_5(AsO_4)_2$ and $Pb_5O_4(CrO_4)$, and Review of PbO-Related Structural Units in Inorganic Compounds. *J. Solid State Chem.* **2004**, *177*, 1321−1332.
(31) Toda, K.; Watanabe, S. Optoelectronic Properties of Pb_5CrO_8 Thin Films for Application to Contact-Type Line-Image Sensor. *J. Appl. Phys.* **1995**, *77*, 2786.
(32) Lee, J.; Ye, H.; Pan, S.; Bard, A. J. Screening of Photocatalysts by Scanning Electrochemical Microscopy. *Anal. Chem.* **2008**, *80*, 7445−50.
(33) Bhattacharya, C.; Lee, H. C.; Bard, A. J. Rapid Screening by Scanning Electrochemical Microscopy (SECM) of Dopants for Bi_2WO_6 Improved Photocatalytic Water Oxidation with Zn Doping. *J. Phys. Chem. C* **2013**, *117*, 9633.
(34) Newhouse, P. F.; Parkinson, B. A. Combinatorial Optimization of Spinel $Co_{3-x}M_xO_4$ M = (Al, Ga, In) Alloyed Thin Films Prepared by Ink Jet Printing: Photoelectrochemical, Optical, and Structural Properties. *J. Mater. Chem. A* **2015**, *3*, 5901.
(35) Storm, S. L.; Springsteen, A.; Ricker, T. M. *Lab Sphere Application Note*; 1998; pp 1−8.
(36) van de Krol, R. In *Photoelectrochemical Hydrogen Production (Electronic Materials: Science & Technology)*; van de Krol, R.; Grätzel, M., Eds.; Springer: New York, 2012; Vol. *102*, pp 13−68.
(37) Tauc, J.; Grigorovici, R.; Vancu, A. Optical Properties and Electronic Structure of Amorphous Germanium. *Phys. Status Solidi B* **1966**, *15*, 627−637.
(38) Araújo, V. D.; Andreeta, M. R. B.; Maia, L. J. Q.; Nascimento, R. M.; Motta, F. V.; Bomio, M. R. D.; Paskocimas, C. A.; Bernardi, M. I. B. Microstructural, Structural and Optical Properties of Nanoparticles of PbO-CrO_3 Pigment Synthesized by a Soft Route. *Ceramica* **2015**, *61*, 118−125.
(39) Searson, P. C.; Latanision, R. M. Analysis of the Photoelectrochemical Response of the Passive Film on Iron in Neutral Solutions. *J. Electrochem. Soc.* **1988**, *135*, 1358−1363.
(40) Bard, A. J.; Faulkner, L. R. *Electrochemical Methods: Fundamentals and Applications*, 2nd ed.; John Wiley & Sons: New York, 2001; p 833.
(41) Quareni, S.; De Pieri, R. A Three-Dimensional Refinement of the Structure of Crocoite, $PbCrO_4$. *Acta Crystallogr.* **1965**, *19*, 287−289.
(42) Bandiello, E.; Errandonea, D.; Martinez-Garcia, D.; Santamaria-Perez, D.; Manjón, F. Effects of High-Pressure on the Structural, Vibrational, and Electronic Properties of Monazite-Type $PbCrO_4$. *Phys. Rev. B: Condens. Matter Mater. Phys.* **2012**, *85*, 024108.
(43) Stoltzfus, M. W. Structure-Property Relationships in Solid State Materials: a Computational Approach Emphasizing Chemical Bonding. Ph.D. Thesis, Ohio State University, 2007.
(44) Chun, W. − J.; Ishikawa, A.; Fujisawa, H.; Takata, T.; Kondo, J. N.; Hara, M.; Kawai, M.; Matsumoto, Y.; Domen, K. Conduction and Valence Band Positions of Ta_2O_5, TaON, and Ta_3N_5 by UPS and Electrochemical Methods. *J. Phys. Chem. B* **2003**, *107*, 1798−1803.
(45) Liu, G.; Jaegermann, W.; He, J.; Sundström, V.; Sun, L. XPS and UPS Characterization of the TiO_2/ZnPcGly Heterointerface: Alignment of Energy Levels. *J. Phys. Chem. B* **2002**, *106*, 5814−5819.
(46) Resasco, J.; Zhang, H.; Kornienko, N.; Becknell, N.; Lee, H.; Guo, J.; Briseno, A. L.; Yang, P. $TiO_2/BiVO_4$ Nanowire Heterostructure Photoanodes Based on Type II Band Alignment. *ACS Cent. Sci.* **2016**, *2*, 80−88.

DOI: 10.1021/acs.jpcc.7b03230
J. Phys. Chem. C 2017, 121, 17561−17568